Available online at
www.ijacskros.com

Indian
Journal of Advances in
Chemical Science

Indian Journal of Advances in Chemical Science 4(3) (2016) 241-249

Crystallographic and Morphological Study of Barium Substituted Sodium Zirconium Phosphate: $Na_{1-x}Ba_{x/2}Zr_2P_3O_{12}$ (x=0.1-1.0)

Rashmi Chourasia*, O. P. Shrivastava, Vijay Verma

Department of Chemistry, Dr. H.S. Gour University, Sagar - 470 003, Madhya Pradesh, India.

Received 19th April 2016; Revised 25th May 2016; Accepted 30th May 2016

ABSTRACT

Sodium zirconium phosphate (NZP) is a potential material for immobilization of nuclear effluents. The existence of barium containing NZP structure was determined on the basis of crystal data of solid state simulated waste forms. The crystal chemistry of $Na_{1-x}Ba_{x/2}Zr_2P_3O_{12}$ (x=0.1-1.0) has been investigated using general structure analysis system programing. The barium NZP phases crystallize in the space group R-3c and Z=6. Powder diffraction data have been subjected to Rietveld refinement to arrive at a satisfactory structural convergence of R-factors. The unit cell volume and polyhedral (ZrO_6 and PO_4) distortion increase with rise in the mole % of Ba^{2+} in the NZP matrix. Scanning electron microscopy, transmission electron microscopy, and energy dispersive X-ray analysis provide analytical evidence of barium in the matrix.

Key words: *Ceramic, Barium sodium zirconium phosphate, Powder X-ray diffraction, General structure analysis system, Rietveld refinement, Nuclear waste immobilization.*

1. INTRODUCTION

The disposal of high-level radioactive waste generated during reprocessing of spent fuel from nuclear reactors to recover actinides is a research problem of interest to nuclear scientists. Chemically and radiologically, reprocessed wastes are extremely complex in nature [1]. They contain fission products, residual actinides, cations from dissolution of fuel rod containers, alkali salts, and a variety of organic compounds. To reduce their volume and to stabilize their chemistry, reprocessed commercial wastes in liquid form are often converted into solid form by drying and calcining them at temperatures below 600°C. During calcination, the wastes decompose into amorphous mixtures of chemically inert oxides while volatile reaction products are driven off. The solid products or calcines are characterized by moderate to high leachability and need to be converted to chemically stable form before they are finally disposed off. As a result, the development of waste forms that are suitable for immobilization of reprocessed high-level calcines have continued to remain a challenging task for chemists. In response to this challenge, a variety of waste forms including non-crystalline borosilicate glasses [2], crystalline, and multiphase materials have been proposed. One of them is the sodium zirconium phosphate (hereafter NZP), which allows accommodation of cations of various size and oxidation states on three distinct crystallographic sites, in fact, all chemical species associated with reprocessed commercial high-level waste calcines may be crystallochemically accommodated in NZP matrix [3,4]. Literature indicates that the NZP waste forms are highly resistant to radiation damage. As crystalline waste forms, NZP compounds offer inherently low leach rate for single phases, negligible thermal expansion, and ability to immobilize high concentration of waste in high-density phases [5-9]. These characteristics of waste forms render these materials promising candidate for disposal of nuclear effluents. Being high-density crystalline material, it offers a notable economic advantage over less dense and thermodynamically unstable borosilicate based glasses.

The crystal structure of NZP can be described as a network formed by the corner sharing of PO_4 tetrahedra and ZrO_6 octahedra. The basic unit consists of two MO_6 octahedra and three PO_4 tetrahedra, which are linked along c-axis. Such ribbons along the c-axis are interconnected by PO_4 tetrahedral units along the a-axis. The articulation of these ribbons and chains creates structural holes or interstitial sites in the structure which can accommodate a variety of ions. There are four such sites per formula unit of NZP, as represented by the crystallographic formula (A_I) $(A_{II})_3M_2(PO_4)_3$. The A_I and A_{II} sites have different crystallographic

*Corresponding Author:
E-mail: dr.rchourasia@gmail.com

orientations. The A_I site is situated between two MO_6 octahedra along the c-axis with a distorted octahedral coordination, while A_{II} site is located between the ribbons with 8-fold coordination. In NZP, Na ion occupies only the type I (*6b*) sites, whereas type II (*18e*) sites remain empty. The rigid framework structure allows either no occupancy as in $NbTiP_3O_{12}$ or partial occupancy as in NZP and NaSicon ($Na_3Zr_2Si_2PO_{12}$). Thus, NZP offers an open structure with the rigid framework and vacant interstitial sites which can be filles by metal ions. The NZP structure is versatile in that chemical substitution is possible at the A, M, and P sites by a variety of elements to give rise to large number of isostructural phases including vacancy at the A site [10-12]. The substitution at the A site includes alkali and alkaline earth metals, transition metals, and rare earth metals. The zirconium sites can be occupied by tri, tetra, and pentavalent ions. Fission products and other actinides also substitute for zirconium as essential constituents of the three-dimensional (3D) network. In this context, several authors have reported their findings on various routes of synthesis and scientific data on corresponding simulated, mono, and multielement waste forms [13-18]. Besides identifying the limit of barium loading, present communication demonstrates the scientific feasibility of barium immobilization in the NZP matrix through an acceptable structure model based on the refinement of crystallographic data. It also investigates the crystallochemical changes due to matrix modification when a large cation-like Ba^{2+} is substituted for sodium on A_I site of the NZP framework.

2. EXPERIMENTAL

2.1. Ceramic Route Synthesis of $Na_{1-x}Ba_{x/2}Zr_2P_3O_{12}$ Phases

Calculated quantities of AR grade Na_2CO_3, $BaCO_3$, ZrO_2 and $(NH_4)H_2PO_4$ for the stoichiometry $Na_{1-x}Ba_{x/2}Zr_2P_3O_{12}$ (x=0.1, 0.5 and 1) were thoroughly mixed with about 10 ml of 1, 2, 3 propanetriol to form a semisolid paste. The glycerol paste was gradually heated initially at 600°C for 4 h in a crucible. This initial heating is done to decompose Na_2CO_3 and $(NH_4)H_2PO_4$ with emission of carbon dioxide, ammonia, and water vapors. The mixture was reground to micron size, pressed into pellets, and sintered in a platinum crucible at 1200°C for 12 h. The process was repeated to get a polycrystalline dense material.

2.2. Characterization

The powder X-ray diffraction (XRD) pattern has been recorded between 2θ=10°-90° on a Pan Analytical diffractometer (XPERT-PRO) using CuKα radiation at step size of 2θ=0.017° and a fixed counting time of 5 s/step. Scanning electron microscopy (SEM) has been carried out on an electron microscope system (HITACHI S-3400) equipped with Thermonoran ultra dry detector facility for energy dispersive X-ray (EDX) analysis. Transmission electron microscopy (TEM) study was done with a PHILIPS CM200 analytical instrument operated between 20 and 200 kV.

3. RESULTS AND DISCUSSION

3.1. Rietveld Refinement and Crystallographic Model of the Phases

XRD data show that solid solution of compositions $Na_{1-x}Ba_{x/2}Zr_2P_3O_{12}$ (x=0.1 and 0.5) are isostructural to $NaZr_2(PO_4)_3$ [19] although in case of x=0.5, a minor secondary phase of barium zirconium phosphate (*marked) begins to appear along with $NaZr_2(PO_4)_3$ (Figure 1). Barium sodium zirconium phosphate (BaNZP) crystallizes in the rhombohedral system (x=0.1, 0.5 in R-3c space group, whereas x=1.0 in R-3). The conditions for the rhombohedral lattice: (i) - h+k+l=3n, (ii) when h=0, l=2n, and (iii) when k=0, l=2n have been verified for all reflections between 2q=10°-90°. The intensity and positions of the diffraction pattern match with the characteristic pattern of parent compound NZP, which gives several prominent reflections between 2q=13.98°-46.47° [19]. The Rietveld [20] refinement of the step scan data was performed by the least square method using GSAS software [21]. Assuming that BaNZP belongs to the Nasicon family, Zr, P, and O atoms are in the *12c*, *18e,* and *36f* Wyckoff positions, respectively of the R-3c space group. In BaNZP phases, the Na atoms were assumed to occupy the M_1 (*6b*) site while M_2 site (*18e*) remains vacant. The occupancies of Na and Ba atoms have been constrained according to their theoretical molar ratios. The structure refinement leads to rather good agreement between the experimental and calculated XRD pattern (Figure 2) and yields acceptable reliability factors: R_f^2, R_p and R_{wp} (Table 1) [22]. The normal probability plot for the histogram gives nearly a linear relationship indicating that the I_o and I_c values, for the most part, are normally distributed.

The 3D network structure of NZP consists of strongly bonded polyhedra, which imparts stability. The structure is flexible toward ionic substitutions on

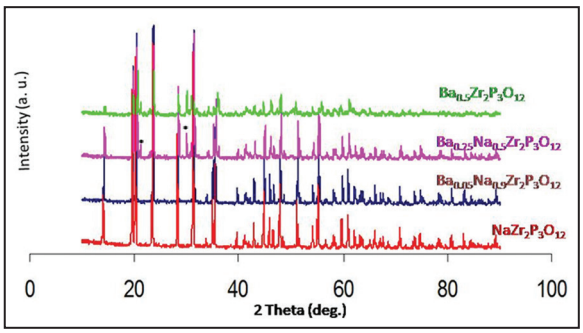

Figure 1: Powder X-ray diffraction pattern of $Na_{1-x}Ba_{x/2}Zr_2P_3O_{12}$ (x=0.1-1.0) ceramic samples. Marked (*) are due to secondary phase of barium zirconium phosphate.

Table 1: Crystallographic data for $Na_{1-x}Ba_{x/2}Zr_2P_3O_{12}$ (x=0.1-1.0) phases.

Structure	Rhombohedral	Z	6
Space group	R-3c	α=β=	90°
		γ=	120.0°
Parameters	X=0.1	X=0.5	X=1.0
Lattice constants			
a=b	8.79326 (7)	8.80260 (30)	8.7355 (9)
c	22.72401 (30)	22.7666 (14)	23.268 (5)
R_p	0.0949	0.1469	0.1854
R_{wp}	0.1238	0.1966	0.2442
$R_{expected}$	0.0681	0.0697	0.0788
R_F^2	0.08351	0.16872	0.20601
Volume of unit cell	1521.652 (21)	1527.74 (9)	1537.7 (4)
S (GoF)	1.82	2.83	
DWd	0.832	0.431	0.241
Unit cell formula weight	2969.445	3079.065	3216.09
$Density_{X\text{-}ray}$	3.240	3.347	3.473

$$R_p = \frac{\sum y_i(obs) - y_i(cal)}{\sum y_i(obs)} \quad R_{wp} = \left\{ \frac{\sum w_i(y_i(obs) - y_i(cal))^2}{\sum w_i(y_i(obs))^2} \right\}^2 \quad R_e = \left[(N-9) / \sum w_i y_{oi}^2 \right]^{1/2} \quad S = R_{wp} / R_{exp}$$

. $y_{i(o)}$ and $y_{i(c)}$ are observed and calculated intensities at profile point *i*, respectively. w_i is a weight for each step *i*. *N* is the number of parameters refined

different available sites. The slight increase in lattice parameters may be explained as follows: Lattice parameter "a" depends on the width of the ribbon and on the distance between the ribbons. These quantities are determined by number and size of phosphorus tetrahedrons and substituent cations. Crystal data reveal that the parameter *a* as well as cell volume increases with increasing weight % of substituent cations between the ribbons. This behavior is due to expansion in the rhombohedral lattice caused by the substitution of a smaller Na^+ cation by larger Ba^{2+} cation (Table 1 and Figure 3). Alteration in lattice parameters shows that the network modifies its dimensions to accommodate the cations occupying A_1 site without breaking the bonds. The basic framework of NZP accepts the cations of different sizes and oxidation states to form solid solutions, but at the same time retaining the overall geometry unchanged. The final atomic coordinates and isotropic thermal parameters (Table 2), interatomic distances, bond valences (Table 3), and bond angles (Table 4) are extracted from the crystal information file prepared after final cycle of refinement. Selected h, k, and l values, d-spacing, and intensity data along with observed and calculated structure factors have been listed in Appendix 1. The refinement leads to acceptable Zr–O, P–O bond distances. Zr atoms are displaced from the center of the octahedron due to the Na^+–Zr^{4+} repulsions. Consequently, the Zr–O(2) distance, neighboring the sodium Na(1), is slightly greater than the Zr–O(1) distance; however, average Zr–O distances are smaller than the values calculated

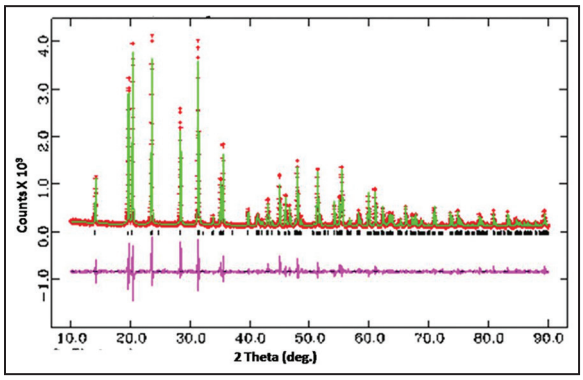

Figure 2: Rietveld refinement plot for $Na_{0.9}Ba_{0.05}Zr_2P_3O_{12}$ ceramic sample showing observed (+), calculated (continuous line), and difference (lower) curves. The vertical bars denote Bragg reflections of the crystalline phases.

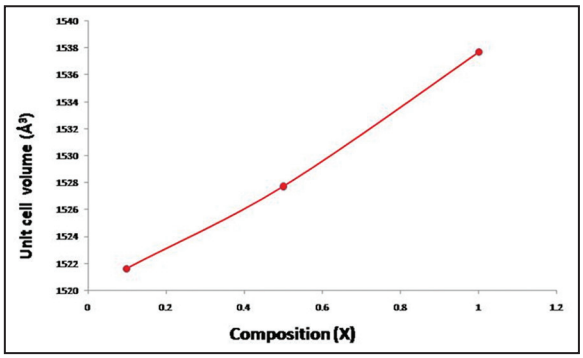

Figure 3: Variation of unit cell volume with Ba loading in the $Na_{1-x}Ba_{x/2}Zr_2P_3O_{12}$ (x=0.1-1.0) solid solutions.

Table 2: Refined atomic coordinates of polycrystalline $Na_{1-x}Ba_{x/2}Zr_2P_3O_{12}$ solid solutions at room temperature.

Atom	x	y	z	Occupancy	$U_{isothermal}$ (Å^2)
$Na_{0.9}Ba_{0.05}Zr_2P_3O_{12}$					
Na	0.0	0.0	0.0	0.9	0.09597
Ba	0.0	0.0	0.0	0.05	0.09597
Zr	0.0	0.0	0.1456	1.0	0.03922
P	0.29111	0.0	0.25	1.0	0.04424
O1	0.17594	−0.02524	0.19628	1.0	0.04387
O2	0.1925	0.1742	0.08889	1.0	0.04387
$Na_{0.5}Ba_{0.25}Zr_2P_3O_{12}$					
Na	0.0	0.0	0.0	0.5	0.25071
Ba	0.0	0.0	0.0	0.25	0.25071
Zr	0.0	0.0	0.1456	1.0	0.04707
P	0.2911	0.0	0.25	1.0	0.04328
O1	0.17594	−0.02524	0.19628	1.0	0.06498
O2	0.1925	0.1742	0.08888	1.0	0.06498
$Ba_{0.5}Zr_2P_3O_{12}$					
Ba	0.0	0.0	0.0	1.0	0.23219
Zr	0.0	0.0	0.1488	1.0	0.06233
Zr	0.0	0.0	0.64577	1.0	0.06233
P	0.2928	0.008	0.2528	1.0	0.07017
O1	0.1971	0.0059	0.1961	1.0	0.13158
O2	0.0429	−0.1673	0.6939	1.0	0.13158
O3	0.183	0.1727	0.084	1.0	0.13158
O4	−0.169	−0.2097	0.5906	1.0	0.13158

Table 3: Interatomic distances (Å) and bond valence variation of polycrystalline $Na_{1-x}Ba_{x/2}Zr_2P_3O_{12}$ ceramic phases.

M–O bond length	$Na_{0.9}Ba_{0.05}Zr_2P_3O_{12}$ (X=0.1)	$Na_{0.5}Ba_{0.25}Zr_2P_3O_{12}$ (X=0.5)	$Ba_{0.5}Zr_2P_3O_{12}$ (X=1.0)
Zr1–O1	2.027910 (10)*3	2.03059 (6)*3	2.02231 (20)*3
Zr1–O2	2.068680 (10)*3	2.07281 (7)*3	
Zr1–O3			2.16638 (27)*3
Zr2–O2			2.01945 (20)*3
Zr2–O4			2.11629 (22)*3
P–O1	1.529830 (10)*2	1.53216 (6)*2	1.55707 (26)
P–O2	1.520700 (10)*2	1.52223 (5)*2	1.54002 (24)
P–O3			1.53008 (15)
P–O4			1.50828 (15)
Na1–O2	2.588220 (20)*6	2.59065 (10)*6	2.58849 (4)*6
Ba–O3			2.4980 (4)*6
Bond valences (V_i)			
Na1	0.81	0.80	
Zr	4.46	4.43	4.10 (Zr1), 4.30 (Zr_2)
P	5.20	5.25	5.09

$V_i=Rb_{ij}$ where $b_{ij}=(R_o/R)$ N. where R is the bond length, N and R_o are constants (N=4.29 and R_o is the value of the bond length for unit bond valence)

from the ionic radii data (2.12 Å) [23]. The O–Zr–O angles vary between 76.90° and 176.3°. The angles implying the shortest bonds are superior to those involving the longest ones due to O–O repulsions which are stronger for O(1)–O(1) than for O(1)–O(2). The P–O distances are close to those found in Nasicon type phosphates.

Figure 4 shows that the PLATON projection of the molecular structure depicting the interlinking of ZrO_6 and PO_4 through a bridge oxygen atom. Figure 5 illustrates that the DIAMOND view showing the ZrO_6 inter-ribbon distance in the structure of the title phase which is a function of amount and size of alkali cation in the A_{II} site of the 3D framework, built from ZrO_6 octahedrons and corner sharing PO_4 tetrahedrons. Substitution of Na^+ by larger cation of Ba^{2+} results in linear increase of distortion in ZrO_6 and PO_4 polyhedra (Figure 6a and b). Calculated valences (Vi) [24], based on bond strength analysis [25,26], are in agreement with the expected oxidation states of Na^+, Zr^{4+}, and P^{5+}, respectively.

Table 4: Interatomic bond angles (deg.) of polycrystalline $Na_{1-x}Ba_{x/2}Zr_2P_3O_{12}$ ceramic phases.

O–M–O bond angles	X=0.1	X=0.5
O2–Na1–O2	65.5678 (7)*6	65.5770 (32)*6
O2–Na1–O2	180.0*3	180*3
O2–Na1–O2	114.4322 (7)*6	114.4230 (32)*6
O1–Zr–O1	90.8995 (6)*3	90.8996 (26)*3
O1–Zr–O2	92.7652 (6)*3	92.8269 (27)*3
O1–Zr–O2	175.8492 (10)*3	175.8069 (10)*3
O1–Zr–O2	90.9229 (6)*3	90.9643 (28)*3
O2–Zr–O2	85.2910 (6)*3	85.1929 (29)*3
O1–P–O1	107.7606 (8)	107.812 (4)
O1–P–O2	108.59470 (10)*2	108.52830 (30)
O1–P–O2	112.7430 (4)*2	112.7932 (17)*2
O2–P–O2	106.4906	106.4736
$Ba_{0.5}Zr_2P_3O_{12}$ (x-1.0)		106.4736
O3–Ba1–O3	65.271 (11)*6	
O3–Ba1–O3	114.729 (11)*6	
O3–Ba1–O3	180.0*3	
O1–Zr1–O1	93.195 (9)*3	
O1–Zr1–O3	92.214 (10)*3,96.793 (10)*3,168.3552 (5)*3	
O3–Zr1–O3	76.903 (11)*3	
O2–Zr2–O2	92.218 (9)*3	
O2–Zr2–O4	176.30580 (30)*3, 90.660 (30)*3, 89.984 (10)*3	
O4–Zr2–O4	87.024 (10)*3	
O1–P–O2	112.503 (13)	
O1–P–O3	108.708 (5)	
O1–P–O4	108.3039 (17)	
O2–P–O3	106.5124 (15)	
O2–P–O4	112.047 (6)	
O3–P–O4	109.28160 (10)	

*Denotes multiplicity

3.2. SEM and TEM Analysis

Within permissible statistical limits, the weight and atomic % of Na, Ba, Zr, P, and O are agreeable with the EDX analysis. In $Na_{0.9}Ba_{0.05}Zr_2P_3O_{12}$, the wt% ratios Ba/Na was found to be 0.18 against the calculated value of 0.13. Likewise, the observed and calculated atomic ratios in this specimen are 0.17 and 0.11, respectively. The EDX spectra provide the evidence of barium in the polycrystalline mono phases while scanning electron micrographs show the rectangular parallelepiped crystallites of varying diameters between 0.5 and 6 mm (Figure 6a and b). In TEM, the nanopowder was observed in the form of

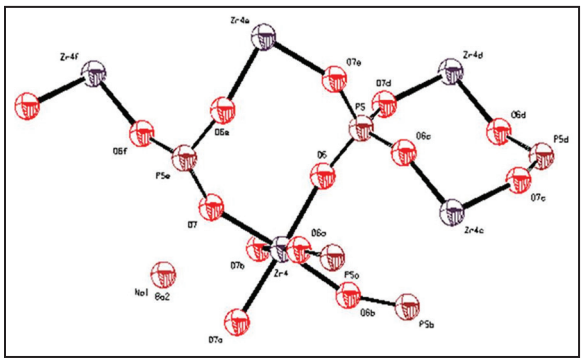

Figure 4: PLATON view of molecular structure of $Na_{0.9}Ba_{0.05}Zr_2P_3O_{12}$ showing Zr coordination in ZrO_6 and P coordination in PO_4 polyhedron at 50% probability level.

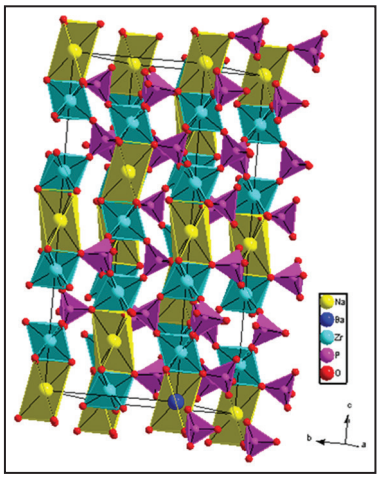

Figure 5: DIAMOND projection of crystal structure of $Na_{0.9}Ba_{0.05}Zr_2P_3O_{12}$ ceramic phase.

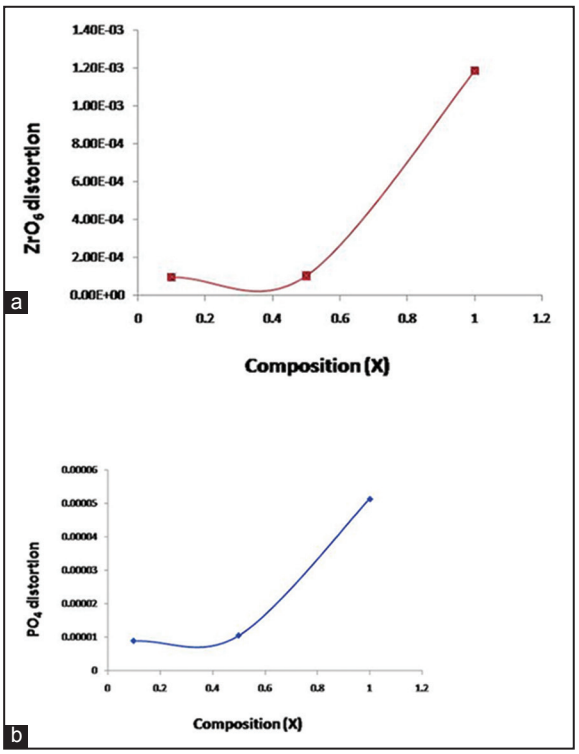

Figure 6: (a and b) Variation of polyhedral distortions in Na_{1-x} $Ba_{x/2}Zr_2P_3O_{12}$ solid solutions with barium loading.

Table 5: Distribution of particle size (nm) along prominent reflecting planes of $Na_{1-x}Ba_{x/2}Zr_2P_3O_{12}$ ceramic samples.

h, k, l	X=0.1	X=0.5	X=1.0
1, 0, −2	119.7	119.8	119.7
1, 0, 4	80.4	96.5	68.9
1, 1, 0	96.6	96.6	69.0
0, 0, 6	69.4	80.9	80.9
2, 0, −4	98.1	98.1	70.0
1, 1, 6	123.4	123.4	61.8
2, 1, 4	99.7	124.7	99.8
3, 0, 0	124.8	124.8	83.2
3, 0, −6	166.6	125.07	63.4
2, 1, −8	105.4	140.6	128.5
3, 1, −4	141.1	105.8	73.8
2, 1, −10	141.5	141.5	64.8
2, 2, 6	85.3	106.7	104.1
2, 1, 10	108.1	108.1	21.9
3, 1, 8	87.5	109.5	66.7
3, 2, 4	109.9	109.9	67.1
4, 1, 0	109.5	146.8	67.1
3, 1, −10	150.0	149.9	91.2
2, 0, 14	115.6	77.1	70.5

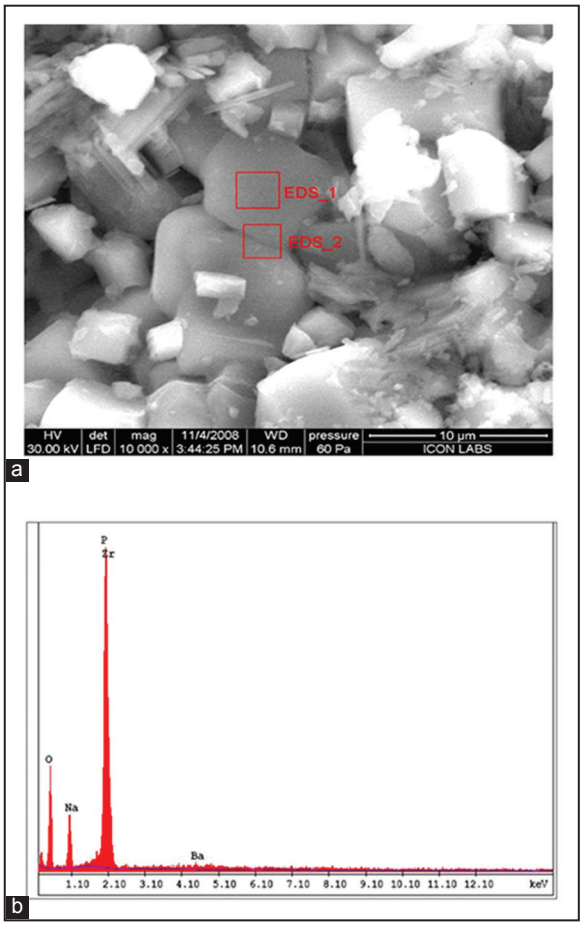

Figure 7: (a) Scanning electron micrographs and (b) energy dispersive X-ray analysis spectrum of $Na_{0.9}Ba_{0.05}Zr_2P_3O_{12}$ ceramic phase.

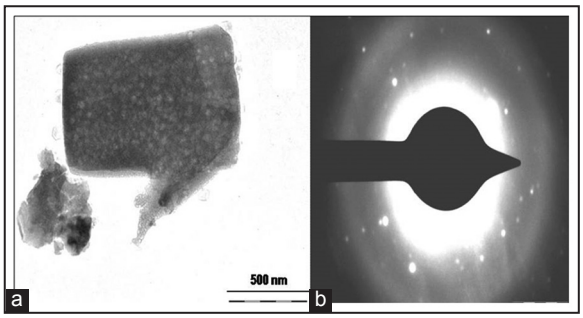

Figure 8: (a) Transmission electron microscopy image of the bulk nano phase of $Na_{0.9}Ba_{0.05}Zr_2P_3O_{12}$ (b) selected area electron diffraction image of $Na_{0.9}Ba_{0.05}Zr_2P_3O_{12}$ polycrystalline powder showing the fundamental reflections.

agglomerates (Figure 7a). Simultaneously, the particle size was also determined using the Scherrer's equation where broadening of peak is expressed as the full width at half maxima in the recorded XRD pattern [24] (Table 5). The selected area electron diffraction pattern of nano ceramic shows concentric rings in the diffraction pattern, which confirms the polycrystalline

nature of the ceramic powder. Crystallographic planes and ordered arrangement of atoms are visible in the electron microscopy image (Figure 7b).

4. CONCLUSIONS

Refinement of powder XRD data shows that the solid solutions of BaNZP crystallize in the rhombohedral system (x=0.1, 0.5 in R-3c space group, whereas x=1.0 in R-3). The Rietveld plots represent a good structure fit between observed and calculated intensity with satisfactory R-factors. The bond distances Zr–O, P–O, and Na–O are in agreement with their corresponding values for respective oxides. Cell volume and bond distortions in ZrO_6 and PO_4 polyhedra vary linearly with barium loading, but the overall structure of the matrix remains intact. NZP has been identified as a potential material for immobilization and solidification of barium.

5. ACKNOWLEDGMENT

Authors are thankful to Professor J. P. Shrivastava, Department of Geology, Delhi University, India, for SEM/EDAX analysis and the Department of Metallurgical Engineering and Material Science I.I.T. Bombay, India, for XRD analysis. One of the authors (Dr. Rashmi Chourasia) is grateful to UGC, New Delhi, India, for the award of Women Post Doctoral Fellowship.

6. REFERENCES

1. H. T. Hawkins, B. E. Scheetz, (1996) Preparation of Mono Phasic Sodium Zirconium Phosphate (NZP) Radiophases: Potential Host Matrix for the Immobilization of Reprocessed Commercial High-Level Wastes, ***Proceedings of the Material Research Society*, *Fall Meeting,*** Boston, MA, December, 2-6.
2. A. E. Ringwood, S. E. Kesson, N. G. Ware, W. Hibberson, (1979) Geological immobilization of nuclear reactor wastes, ***Nature,* 278:** 219.
3. V. I. Pet'kov, M. V. Sukhanov, (2003) Immobilization of molybdenum from fuel reprocessing wastes into sodium zirconium phosphate ceramics, ***Czechoslovak Journal of Physic,* 53:** A671.
4. J. Alamo, (1993) Chemistry and properties of solids with [NZP] skeleton, ***Solid State Ionics*, 63-65:** 547-561.
5. V. I. Petkov, A. I. Orlova, (2003) Crystal-chemical approach to predicting the thermal expansion of compounds in the NZP family, ***Inorganic Materials,* 39(10):** 1013-1023.
6. G. Buvaneswari, K. V. Govindan Kutty, U. V. Varada-Raju, (2004) Thermal expansion behaviour of sodium zirconium phosphate structure type phosphates containing tin, ***Materials Research Bulletin,* 39:** 475.
7. R. Roy, L. J. Yang, J. Alamo, E. R. Vance, (1983) In: D. J. Brookins, (Ed.), ***Scientific Basis for Nuclear Waste Management** – VI*, Amsterdam: North-Holland.
8. A. H. Naik, N. V. Thakkar, S. R. Dharwadkar, K. D. S. Mudher, V. Venugopal, (2004), ***Journal of Thermal Analysis and Calorimetry*, 78:** 707-713.
9. W. Lutze, R. C. Ewing, (1988) ***Radio Active Waste for the Future,*** Amsterdam: Elsevier Science Publication, p238.
10. F. J. Berry, N. Costantini, L. E. Smart, (2006) Synthesis and characterisation of Cr^{3+}-containing NASICON-related phases, ***Solid State Ionics*, 177:** 2889-2896.
11. A. El Jazouli, J. L. Souberoux, J. M. Dance, L. Flem, (1986) The nasicon like Cu-II titanium phosphate $Cu_{0.50}Ti_2(PO_4)_3$, ***Journal of Solid State Chemistry,* 65:** 351.
12. J. L. Rodrigo, J. Alamo, (1991) Phase transition in $NaSn_2(PO_4)_3$ and thermal expansion of Na $M^{IV}{}_2(PO_4)_3$ (M^{IV}= Ti, Sn Zr), ***Materials Research Bulletin,* 26:** 475.
13. Y. Hirose, T. Fukasawa, D. K. Agrawal, B. E. Scheetz, R. Nageswaran, J. A. Curtis, S. Y. Limaye, (1999) An alternative process to immobilize intermediate waste from LWR fuel reprocessing. In**: *WM 1999 Conference***.
14. B. E. Scheetz, D. K. Agarwal, E. Breval, R. Roy, (1994) Sodium zirconium phosphate as a host structure for nuclear waste immobilization: A review*, **Waste management*, 14(6):** 489.
15. A. I. Orlova, (2003) Immobilisation of molybdenum from fuel reprocessing wastes into sodium zirconium phosphate ceramics, ***Czechoslovak Journal of Physics*, 53:** Suppl A671.
16. I. W. Donald, B. L. Metcalfe, R. N. J. Taylor, (1997) Review: The immobilization of high level wasre using ceramic and glasses, ***Journal of Materials Science,* 32:** 5851.
17. R. Chourasia, O. P. Shrivastava, R. D. Ambashta, P. K. Wattal, (2010) Crystal chemistry of immobilization of fast breeder reactor (FBR) simulated waste in sodium zirconium phosphate (NZP) ceramic matrix, ***Annals of Nuclear Energy*, 37:** 103-112.
18. R. Chourasia, A. Bohre, R. D. Ambastha, O. P. Shrivastava, P. K. Wattal, (2010) Crystallographic evaluation of sodium zirconium phosphate as a host structure for immobilization of cesium, ***Journal of Materials Science,* 45:** 533-545.
19. JCPDS Powder Diffraction Data File No. 71-0959, (2000) Compiled by ***U.S.A***: ***International Center for Diffraction Data.***
20. H. M. Rietveld, (1969) A profile refinement method for nuclear and magnetic structures, ***J. Journal of Applied Crystallography,* 2:** 65.
21. A. C. Larson, R. B. Von Dreele, (2000) ***General Structure Analysis System Technical Manual, LANSCE, MS-H805,*** Los Almos: National Laboratory LAUR, p86-748.
22. H. Kojitani, M. Kido, M. Akaogi, (2005) Rietveld

analysis of a new high-pressure strontium silicate $SrSi_2O_5$, ***Physics and Chemistry of Minerals*, 32:** 290.
23. R. D. Shannon, C. D. Prewitt, (1969) Effective ionic radii in oxides and fluorides, ***Acta Crystallographica Section B*, 25:** 925-946.
24. A. R. West, (1984) ***Solid State Chemistry and Its Applications*,** New York: John Wiley.
25. R. D. Shannon, C. T. Prewitt, (1970) Revised values of effective ionic radii, ***Acta Crystallographica*, 26:** 1046-1048.
26. N. E. Breese, M. O Keeffe, (1991) Bond-valence parameters for solids, ***Acta Crystallographica*, B47:** 192.

Bibliographical Sketch

Dr Rashmi Chourasia, MSc (Physical chemistry), PhD Publications- 12 International and 04 national, Current Position- UGC Women PDF, Department of Chemistry, Dr H. S. Gour University, Sagar, M. P. India. Dr D. S. Kothari post doctoral fellowship-Dr D. S. Kothari post doctoral fellow at department of Chemistry, Dr H. S. Gour University, Sagar, M. P. India (w. e. f. 27/09/2010 to 27/09/2013). Assistant Professor (Adhoc)- Guru Ghasidas University Bilaspur Chhatishgargh-(w. e. f. 08/07/2010 to 25/09/2010). CSIR Fellowship- Department of Chemistry, Dr H. S. Gour University, Sagar, M. P. India.(w. e. f. 16/09/2009 to 08/07/2010). DST Project Fellow- Department of Chemistry, Dr H. S. Gour University, Sagar M. P. India (w. e. f. 27/04/2007 to 15/09/2009). Life Member of Indian Association of Solid State Chemists and Allied Scientist Jammu, India, LM-358

Appendix 1: Selected h, k, and l values, d-spacing, observed and calculated structure factors and intensity of $Na_{0.9}Ba_{0.05}Zr_2P_3O_{12}$ ceramic phase. The reflection selected from the CIF output of the final cycle of the refinement.

h	k	L	F^2_{Obs}	F^2_{Calc}	d-space	Intensity%
1	0	−2	19750.900	18287.684	6.32579	26.68
1	0	−2	19705.320	18287.684	6.32579	13.25
1	0	4	100894.91	96276.25	4.55351	76.30
1	0	4	98693.73	96276.25	4.55351	37.14
1	1	0	146054.17	146147.91	4.39663	93.92
1	1	0	141860.61	146147.91	4.39663	45.38
1	1	3	92472.18	85376.00	3.80250	100.00
1	1	3	87087.75	85376.00	3.80250	46.98
2	0	−4	157057.80	133768.83	3.16289	60.60
2	0	−4	162213.45	133768.83	3.16289	31.17
1	1	6	144558.28	137704.69	2.86949	99.85
1	1	6	141983.47	137704.69	2.86949	48.85
2	1	1	16422.938	16479.287	2.85546	10.66
2	1	1	16980.049	16479.287	2.85546	5.48
2	1	4	44952.10	41014.15	2.56754	24.21
2	1	4	44558.82	41014.15	2.56754	11.95
3	0	0	163043.14	160796.55	2.53840	42.77
3	0	0	158889.09	160796.55	2.53840	20.77
2	0	8	33574.082	33312.676	2.27675	8.04
1	1	9	12237.561	12853.434	2.18953	6.10
3	0	−6	50855.25	41969.38	2.10860	10.23
3	0	−6	50934.95	41969.38	2.10860	5.10

(Contd...)

Appendix 1: *(Continued)*

h	k	L	F^2_{Obs}	F^2_{Calc}	d-space	Intensity%
2	1	−8	66061.91	55503.40	2.02176	26.49
2	1	−8	64221.23	55503.40	2.02176	12.83
3	1	−4	40672.17	40191.24	1.97968	14.65
3	1	−4	40761.36	40191.24	1.97968	7.32
2	0	−10	54158.29	55099.45	1.95131	10.54
2	0	−10	52056.37	55099.45	1.95131	5.05
2	2	6	97497.90	97520.27	1.90125	35.07
2	2	6	94899.17	97520.27	1.90125	17.02
4	0	−2	29127.232	21005.186	1.87762	5.06
2	1	10	88151.66	88135.33	1.78354	30.30
2	1	10	86470.48	88135.33	1.78354	14.81
3	1	−7	14971.037	16508.191	1.77036	5.06
3	1	8	40181.12	42038.80	1.69489	12.69
3	1	8	34634.492	42038.80	1.69489	5.46
3	2	4	52431.03	49264.69	1.66987	15.48
3	2	4	55045.20	49264.69	1.66987	8.10
4	1	0	108684.36	106767.66	1.66177	31.26
4	1	0	105807.42	106767.66	1.66177	15.17
1	0	−14	59056.25	52011.84	1.58748	9.23
4	0	−8	40586.10	35953.32	1.58145	5.89
3	1	−10	62448.87	66093.79	1.54704	17.78
3	1	−10	59819.32	66093.79	1.54704	8.49
4	1	−6	38107.64	34187.605	1.52173	10.18
4	1	6	37340.63	33495.656	1.52173	9.97
2	0	14	75148.57	80355.43	1.49313	10.90
2	0	14	74247.44	80355.43	1.49313	5.37
5	0	−4	52550.51	52034.19	1.47109	6.66
3	3	0	53553.46	54088.37	1.46554	6.70
4	0	10	49115.77	47492.89	1.45933	6.53
2	1	−14	44987.59	43092.73	1.41383	12.01
2	1	−14	44978.82	43092.73	1.41383	5.99
4	2	−4	23923.008	21494.949	1.39507	5.63
3	2	10	26968.541	27129.773	1.38503	6.49
5	1	4	46479.21	47930.30	1.32973	10.56
5	1	4	45156.61	47930.30	1.32973	5.12
3	1	14	31945.063	33634.938	1.28699	7.45
6	0	0	91596.13	91045.13	1.26920	9.83
5	2	0	27567.639	23630.285	1.21941	5.53
3	2	−14	42234.57	36580.34	1.18913	9.11
5	2	6	26562.545	23945.154	1.16073	5.25
4	3	10	44575.38	38126.73	1.09653	8.54

Intensities less than 5% were omitted. CIF: Crystallographic information framework